

Investigation of the function for buffer layer in coated conductors

Y. WANG^{a,b}, L. ZHOU^{a,b}, Y. F. LU^{b*}, C. S. LI^b, Z. M. YU^b, L. H. JIN^b, J. S. LI^a

^aState Key Laboratory of Solidification Processing, Northwestern Polytechnical University, Xi'an 710072, China

^bNorthwest Institute for Nonferrous Metal Research, Xi'an 710016, China

We have studied the detailed function of $\text{La}_2\text{Zr}_2\text{O}_7$ (LZO) and CeO_2 buffer layer in coated conductors. The results reveal that there is an obvious transformation trend of the orientation for NiO phase from (111) to (00l) in all samples with the increase of oxygen partial pressure in annealing atmosphere. Moreover, it indicates that LZO possesses an effective inhibiting function to the formation of NiO compared with CeO_2 . Therefore, it can be considered that LZO is often fit for being as barrier layer, while CeO_2 is commonly to be as cap layer in multi-layer architecture of buffer layers in coated conductors.

(Received July 10, 2010; accepted August 12, 2010)

Keywords: Coated conductors, Buffer layer, Chemical solution deposition

1. Introduction

The second generation high-temperature superconductors coated conductors, which are very attractive for electrical power application and superconducting, consist of an epitaxial superconducting layer deposited on biaxially textured flexible substrate of a metallic template with buffer layers [1-4]. Buffer layers play a key role in coated conductors. The function of the buffer layers is to prevent the diffusion of metal ions into YBCO, to retard oxidation of metallic substrate, and reduce lattice mismatch between metal substrate and superconducting layer [5]. To date, in order to approve these requirements oxides films with multilayered architecture are commonly adopted to be buffer layers in coated conductors. The typical architecture of multilayered architecture include three-layer architecture consisting of seed, barrier and cap layers for ORNL, and four-layer architecture composing of barrier, nucleation, texture and cap layers for superpower company. So the investigation of the function for buffer layer is very significant to select the appropriate oxides materials to be as the subsidiary functional layers in buffer layers of coated conductors.

Chemical solution deposition (CSD) methods have been used to prepare plenty of oxides films because of their significant cost advantages and nonvacuum circumstance compared to physical vapor deposition (PVD) process [6-9]. Among a series of oxides films prepared by CSD method successfully, $\text{La}_2\text{Zr}_2\text{O}_7$ (LZO) and CeO_2 have been considered as the very promising buffer layers materials. The lattice parameters of LZO with a pyrochlore structure and CeO_2 with a fluorite structure are 3.814 Å and 3.826 Å, respectively. Both

LZO and CeO_2 provide the very small lattice mismatch with the YBCO a- or b-axis ($a = 3.83$ Å and $b = 3.88$ Å). Although the lattice mismatch to NiW ($a = 3.52$ Å) is much higher, LZO and CeO_2 films with good biaxial texture are still obtained on NiW substrate by CSD method [10-15]. We have chosen LZO and CeO_2 as a potential buffer layer for this study. Three kinds of samples with different buffer-layer architecture including single LZO layer (LZO/NiW), single CeO_2 layer (CeO_2/NiW) and both LZO and CeO_2 layers ($\text{CeO}_2/\text{LZO}/\text{NiW}$) are deposited on NiW substrates by CSD methods. Subsequently these crystallized buffer layers and textured NiW substrates are annealed at 900 °C, which is close to the crystallized temperature of YBCO, in oxidation atmosphere with different oxygen partial pressure, respectively. Through investigating the change of texture, structure, composition and morphology between the samples with or without annealing in oxidation atmosphere, the function of $\text{La}_2\text{Zr}_2\text{O}_7$ (LZO) and CeO_2 buffer layer in coated conductors have been studied in detail.

2. Experimental

Three kinds of buffer layers with the same thickness were prepared on NiW substrates by CSD methods. And the CSD precursor solution of LZO and CeO_2 were prepared in ambient atmosphere. Lanthanum (III) acetylacetonate ($\text{La}(\text{acac})_3$), Zirconium (IV) acetylacetonate ($\text{Zr}(\text{acac})_4$) and Cerium (III) acetylacetonate ($\text{Ce}(\text{acac})_3$) were used as received from STREM. For LZO precursor solution, stoichiometric quantities of $\text{La}(\text{acac})_3$ and $\text{Zr}(\text{acac})_4$ were dissolved in

propionic acid by heating and continuous stirring. As such, $\text{Ce}(\text{acac})_3$ was dissolved in propionic acid with the heating and stirring to obtain CeO_2 precursor solution. LZO and CeO_2 precursor solutions were then spin coated onto short cube textured NiW substrates of $1 \text{ cm} \times 1 \text{ cm}$ in size at 2500 rpm for 30 s, respectively. After a 30 minute purge with Ar-4\%H_2 gas mixture at room temperature, the samples were heated at 900 for 1 hour and then quenched to room temperature with the same atmosphere. To CeO_2/LZO double-layer architectures, at the beginning LZO crystallized film was prepared on NiW substrate following the frontal heat treatment process. Then CeO_2 films was deposited on the LZO crystallized film by heat-treated at 900 °C for 1 hour in a flowing mixture of Ar-4\%H_2 gas. Finally, at the end of the crystallized cycles, the above as-prepared samples and the textured NiW substrates were annealed at 900 °C for 1 hour in Ar and Ar-2\%O_2 .

All the samples with or without annealing in oxidation atmosphere were characterized by using X-ray diffraction (XRD), which was performed to carry out θ - 2θ scan by using $\text{CuK}\alpha$ radiation at 40 kV and 50 mA, for crystallinity and epitaxial growth of films. The homogeneity and microstructure of samples were performed by using JSM-6700 field emission scanning electro microscopy (SEM) and the quantitative analysis of the elements on the surface of the samples was done using an Energy Dispersive Spectrometry (EDS).

3. Results and discussion

Fig. 1 shows the θ - 2θ scans of NiW substrate, LZO/NiW, CeO_2/NiW and $\text{CeO}_2/\text{LZO}/\text{NiW}$, which prepared in Ar-4\%H_2 , measured by X-ray diffraction. Except the (002) textured peaks of NiW substrate, the sharp (004) peaks of LZO and (002) peaks of CeO_2 buffer layers are observed. It indicates that the buffer layers have completely crystallized and formed the strong c-axis orientation.

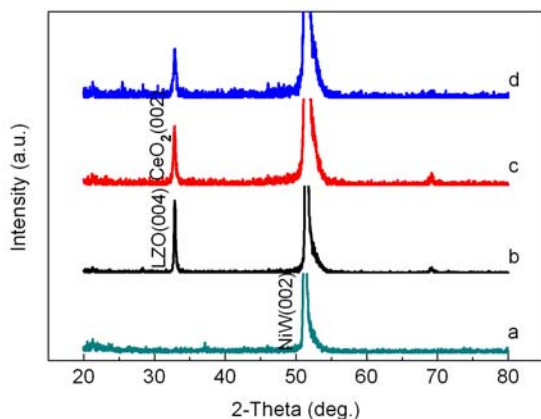


Fig. 1. XRD patterns for (a) NiW substrate, (b) LZO/NiW, (c) CeO_2/NiW and (d) $\text{CeO}_2/\text{LZO}/\text{NiW}$, which prepared in Ar-4\%H_2 .

Figs. 2 and 3 show the XRD θ - 2θ spectrums for NiW, LZO/NiW, CeO_2/NiW and $\text{CeO}_2/\text{LZO}/\text{NiW}$ annealed in

Ar and Ar-2\%O_2 after crystallized in Ar-4\%H_2 , respectively. The oxides polycrystalline related to Ni and W including mainly NiO and NiWO_4 phases are evidence in all samples, at the same time, the LZO (004) and CeO_2 (002) reflection peaks entirely disappear. It illuminates that the texture of buffer layers are completely destroyed along with the oxidation of NiW substrate. It need to be pointed that from XRD spectrums the NiO phase is dominant in LZO/NiW and $\text{CeO}_2/\text{LZO}/\text{NiW}$, while NiWO_4 phase become the main in NiW and CeO_2/NiW whatever they are annealed in Ar or Ar-2\%O_2 . This result may have relation with the different oxidation behavior of NiW substrates in samples with or without buffer layers. The oxidation behavior of NiW substrate is possibly affected by the function of buffer layers. Moreover, there is an obvious transformation trend of the orientation of NiO phase from (111) to (00l) in the samples with buffer layers after annealed in Ar-2\%O_2 . It is possibly because that the oxidation kinetics of metal is generally dependent on its intrinsic structure [16]. Moreover, preferred orientations of NiO grown on the Ni (00l) surface are NiO (111) and NiO (00l), and NiO (00l) becomes dominant at elevated temperatures above 1000 in air [17]. However, it is found that NiO (111) tends to transfer NiO (00l) with the increase of oxygen partial pressure in annealing atmosphere.

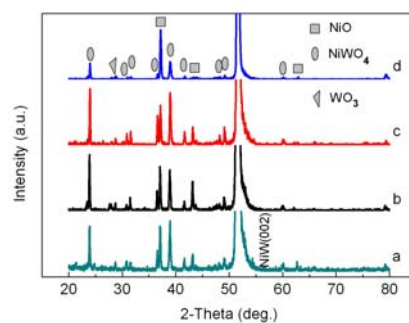


Fig. 2. XRD θ - 2θ spectrums for (a) NiW substrate, (b) LZO/NiW, (c) CeO_2/NiW and (d) $\text{CeO}_2/\text{LZO}/\text{NiW}$ annealed in Ar after crystallized in Ar-4\%H_2 .

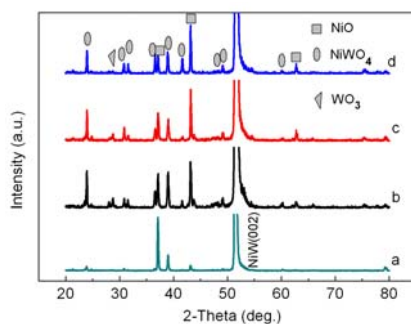


Fig. 3. θ - 2θ scans of (a) NiW substrate, (b) LZO/NiW, (c) CeO_2/NiW and (d) $\text{CeO}_2/\text{LZO}/\text{NiW}$ annealed in Ar-2\%O_2 after crystallized in Ar-4\%H_2 .

Fig. 4 depicts the surface morphology for NiW, LZO/NiW, CeO₂/NiW and CeO₂/LZO/NiW heat-treated in Ar-4%H₂. SEM analysis illustrates smooth, homogeneous and crack-free surfaces of all samples. And the NiW grain boundary grooves on the NiW surface are found to be well covered in LZO/NiW, CeO₂/NiW and CeO₂/LZO/NiW. Average grain size is very different among the latter three samples, the average grains diameter is close to 25 nm for LZO single buffer layer and about 150 nm for CeO₂/LZO double-layers, respectively. It may be because that LZO buffer layer with small oxygen transmittance restrains the growth of oxides related to Ni and W.

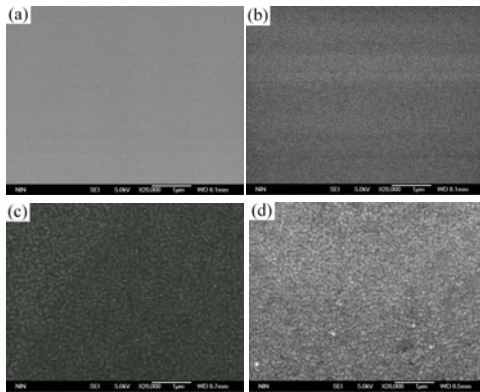


Fig. 4. SEM images for (a) NiW substrate, (b) LZO/NiW, (c) CeO₂/NiW and (d) CeO₂/LZO/NiW, which prepared in Ar-4%H₂.

Figs. 5 and 6 show the SEM images of NiW, LZO/NiW, CeO₂/NiW and CeO₂/LZO/NiW annealed in Ar and Ar-2%O₂ after crystallized in Ar-4%H₂, respectively. However, the surface morphology of all samples annealed in oxidation atmosphere is completely different from that of the as-grown samples. It is clear that the abnormal grains upgrowth appears on the surface of samples due to the oxidation of NiW substrates, which is confirmed by the XRD patterns. It displays a rough, porous with diameters ~ 300 nm microstructure for NiW substrate after annealed in Ar. While the X-ray diffraction patterns indicated the formation of NiWO₄ and NiO polycrystalline phases, the surface roughness and porosity may result from the oxidation of NiW substrate in a low oxygen partial pressure, which is approximate with slow oxygen penetration process. For LZO/NiW annealed in Ar, plenty of round grains with diameters ~ 200 nm are found and larger rhombic grains, of which diameter reach to about 1 μm, appear at local sites on the surface of sample. However, a large number of spiculate grains with diameters ~ 1 μm are formed on the surface of CeO₂/NiW annealed in Ar. It is very interesting that larger rhombic grains with diameters ~ 900 nm, which is very similar to the large grains on the local sites of LZO/NiW sample annealed in Ar, are observed on the surface of CeO₂/LZO/NiW and the separation of these grains is about 1 μm. It illuminates that the morphology of CeO₂/LZO/NiW annealed in non-reducing atmosphere

is highly influenced by the existence of LZO buffer layer.

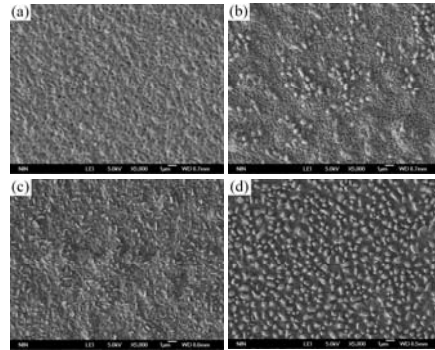


Fig. 5. SEM micrographs for (a) NiW substrate, (b) LZO/NiW, (c) CeO₂/NiW and (d) CeO₂/LZO/NiW annealed in Ar after crystallized in Ar-4%H₂.

For NiW substrate annealed in Ar – 2% O₂, the film consists of petal shaped drapes with diameters ~ 1 μm on its surface. The formation of this continuous film may be resulting from the augment of oxidation rate of NiW substrate with the increase of oxygen partial pressure. A large number of rhombic grains with ~ 300 nm are observed uniformly on the surface of LZO/NiW annealed in Ar-2% O₂. Similar surface morphologies are observed for CeO₂/LZO/NiW annealed in Ar-2%O₂ except its larger surface roughness than that of former. However, a mass of spiculate grains with diameters ~ 1.5 μm are again detected on the surface of CeO₂/NiW annealed in Ar-2%O₂. In fact, the grains of NiWO₄ and NiO should usually be spherical-shaped [18]. Therefore the phenomenon that rhombic-shaped and spiculate grains are obtained on the surface of the samples annealed in oxidation atmosphere may be attributed to the mutual squeeze due to competitive growth process among these oxides of Ni and W with different nucleation energy through crystallized buffer layers and different oxides grains orientation.

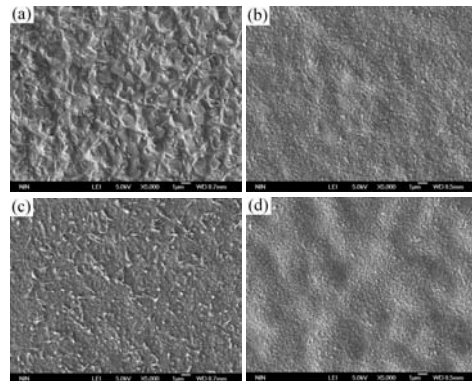


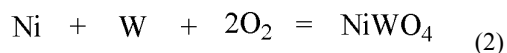
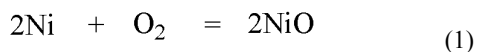
Fig. 6. SEM images of (a) NiW substrate, (b) LZO/NiW, (c) CeO₂/NiW and (d) CeO₂/LZO/NiW annealed in Ar-2%O₂ after crystallized in Ar-4%H₂.

The X-ray diffraction patterns of Figs. 2 and 3 indicate that NiWO₄ and NiO are the main oxidation productions of NiW substrate in NiW, LZO/NiW, CeO₂/NiW and CeO₂/LZO/NiW either annealed in Ar or Ar-2%O₂. But the content of NiWO₄ and NiO are very different in all samples annealed in the same oxidation atmosphere and in one sample annealed in different oxygen partial pressure. The ratios of these oxides, which are computed by dividing the molar percentage of NiWO₄ by that of NiO, are listed in Table 1 by the analysis of EDS results of the samples annealed in Ar and Ar – 2% O₂. It is clear that the content of NiO is much larger than that of NiWO₄, and this phenomenon becomes more evident with the increase of oxygen partial pressure in annealing atmosphere. In addition, the ratios of these oxides in NiW and CeO₂/NiW are always larger than that in LZO/NiW and CeO₂/LZO/NiW after annealed in non-reducing atmosphere.

Table 1. The ratios of the oxides (computed by dividing the molar percentage of NiWO₄ by that of NiO) in all samples annealed in oxidation atmosphere.

atmosphere	NiW	LZO/NiW	CeO ₂ /NiW	CeO ₂ /LZO/NiW
Ar	124.08	16.27	38.63	24.15
Ar-2%O ₂	686.86	267.33	540.33	441.55

It can be speculated that two chemical reactions of NiW substrate listed as below take place in samples annealed in non-reducing atmosphere. The Gibbs free energy change of reaction (1) and (2) are calculated to be -264.317 KJ•mol⁻¹ and -717.971 KJ•mol⁻¹ at the annealing temperature of 900 °C, respectively. It illuminates that reaction (2) is easier to be taken place than reaction (1) because of the smaller Gibbs free energy change of former than that of latter. Because the content of 95%Ni and 5%W in NiW substrate result in the larger content of NiO than that of NiWO₄ in samples after annealed in oxidation atmosphere. Moreover, the ability of their against oxygen diffusion of different buffer layers play a key role in the difference of the ratios of NiWO₄ and NiO.



From the XRD, SEM and EDS analysis, the formation of plentiful NiO grains with c-axis orientation results in the grains refinement on the surface of samples annealed in Ar-2%O₂. It is highly possible that the grater nucleation density of NiW oxides leads to the smaller grains granularity and the growth of oxides film may be easily induced by the cube-texture of NiW substrate to form orientation film at the higher oxygen partial pressure. The content of NiO increases, while that of

NiWO₄ decreases when the Ar-2%O₂ is instead of Ar in annealing atmosphere. It indicates that the effect of oxygen partial pressure on the formation of NiO is larger than on that of NiWO₄. It can be considered that rhombic grains are observed on the surface of samples annealed in oxidation atmosphere when the buffer layers include LZO, while spiculate grains appear on the surface of samples annealed in oxidation atmosphere only when CeO₂ is applied as single buffer layer. Furthermore, The similar morphology between LZO/NiW and CeO₂/LZO/NiW are very different from the morphology of CeO₂/NiW after annealed in the same atmosphere, illuminating that their morphology character are mainly influenced by existence of LZO. The content of oxides related to Ni and W in LZO/NiW and CeO₂/LZO/NiW is less than that in NiW and CeO₂/NiW annealed in the same oxidation atmosphere, indicating that LZO displays an effective inhibiting function to the formation of NiO although its ability against oxygen diffusion is limited. However, the content of the oxides in CeO₂/NiW is very close to that in NiW after annealed in the same oxidation atmosphere, and to CeO₂/NiW, the influence of oxygen partial pressure on its morphology and the content of oxides related to Ni and W is not great, which suggests that CeO₂ film performs a bad protection against oxygen diffusion. Therefore, LZO is propitious to be adopted as barrier layer in multilayer architecture of buffer layers, but CeO₂ is fit for being as cap layer because of its smaller lattice mismatch with YBCO film.

4. Conclusions

We have studied the function of buffer layers in coated conductors by investigating the change of texture and morphology of all samples with different buffer layers architecture with or without annealing in oxidation atmosphere. It reveals that there is an obvious transformation trend of the orientation of NiO phase from (111) to (00l) in all samples with the increase of oxygen partial pressure in annealing atmosphere. And LZO displays an effective inhibiting function to the formation of NiO. The results indicate that LZO with small intrinsic oxygen transmittance is often fit for being as barrier layer and CeO₂ with great intrinsic oxygen transmittance is commonly to be as cap layer in multi-layer architecture of buffer layer in coated conductors. It also illuminates that buffer layers with small intrinsic oxygen transmittance may weaken the oxidation of NiW substrate, which is beneficial to the transfer of texture from NiW to superconducting layer.

Acknowledgements

This work was financially supported by the National Science Fund Program and National 863 Program of China (Grant No. 50872115 and 2006AA03Z204).

References

- [1] D. Larbalestier, A. Gurevich, D. M. Feldmann, A. Polyanskii, *Nature* **414**, 368 (2001).
- [2] M. W. Rubich, U. Schoop, D. T. Verebelyi, C. Thieme, W. Zhang, in *Applied Superconductivity Conference*, Houston Texas, 2002.
- [3] A. H. Robert, K. C. David, *Physica C* **445**, 488 (2006).
- [4] V. Selvamanickam, Y. Chen, X. Xiong, Y. Xie, X. Zhang, Y. Qiao, J. Reeves, A. Rar, R. Schmidt, K. Lenseth, *Physica C* **463**, 482 (2007).
- [5] L. Arda, S. Ataoglu, S. Sezer, Z. Abdulaliyev, *Surface & Coatings Technology* **202**, 439 (2007).
- [6] M. S. Bhuiyan, M. Paranthaman, K. Salama, *Supercond. Sci. Technol.* **19**, R1 (2006).
- [7] X. Obradors, T. Puig, A. Pomar, F. Sandiumenge, S. Pinol, N. Mesters, O. Castaño, M. Coll, A. Cavallaro, A. Palau, J. Gázquez, J. C. Gonzalez, J. Gutiérrez, N. Romà, S. Ricart, J. M. Moretó, M. D. Rossell, G. V. Tendeloo, *Supercond. Sci. Tech.* **17**, 1055 (2004).
- [8] S. Engel, K. Knoth, R. Hühne, L. Schultz, B. Holzapfel, *Supercond. Sci. Technol.* **18**, 1385 (2005).
- [9] M. P. Paranthamana, M. S. Bhuiyan, S. Sathyamurthy, *Physica C* **468**, 1587 (2008).
- [10] K. Knoth, R. Hühne, S. Oswald, L. Schultz, B. Holzapfel, *Supercond. Sci. Technol.* **18**, 334 (2005).
- [11] T. Caroff, S. Morlens, A. Abrutis, M. Decroux, P. Chaudouët, L. Porcar, Z. Saltyte, C. Jiménez, P. Odier, F. Weiss, *Supercond. Sci. Technol.* **21**, 1 (2008).
- [12] K. Knoth, R. Hühne, S. Oswald, L. Molina, O. Eibl, L. Schultz, B. Holzapfel, *Thin Solid Films* **516**, 2099 (2008).
- [13] M. S. Bhuiyan, M. Paranthaman, S. Sathyamurthy, T. Aytug, S. Kang, D. F. Lee, A. Goyal, E. A. Payzant, K. Salama, *Supercond. Sci. Technol.* **16**, 1305 (2003).
- [14] S. S. Wang, Z. Han, W. Schmidt, H. W. Neumuller, P. Du, L. Wang, S. Chen, *Supercond. Sci. Technol.* **18**, 1468 (2005).
- [15] B. Rousseau, S. Phok, L. Ortega, N. Guibadj, T. Wegelius, S. Morlens, P. Odier, F. Weiss, J. Eikmeyer, *Journal of the European Ceramic Society* **25**, 2185 (2005).
- [16] T. Homma, N. N. Khoi, W. W. Smeltzer, J. D. Embury, *Oxidation of Metals* **3**, 463 (1971).
- [17] T. Watanabe, K. Matsumoto, T. Maeba, T. Tanigawa, I. Hirabayashi, *Physica C* **357**, 914 (2001).
- [18] A. Kuzmin, J. Purans, R. Kalendarev, D. Pailharey, Y. Mathey, *Electrochimica Acta* **46**, 2233 (2001).

*Corresponding author: wyspacestar@yahoo.com.cn